Neuroretinal Rim Response to Transient Intraocular Pressure Challenge Predicts the Extent of Retinal Ganglion Cell Loss in Experimental Glaucoma

Nimesh B. Patel, Louvenia Carter-Dawson, and Laura J. Frishman

University of Houston College of Optometry, Houston, Texas, United States

Correspondence: Nimesh Patel, University of Houston College of Optometry, 4401 Martin Luther King Blvd., Houston, TX 77204, USA; npatel@central.uh.edu.

Received: December 13, 2022
Accepted: May 12, 2023
Published: May 31, 2023

Citation: Patel NB, Carter-Dawson L, Frishman LJ. Neuroretinal rim response to transient intraocular pressure challenge predicts the extent of retinal ganglion cell loss in experimental glaucoma. *Invest Ophthalmol Vis Sci.* 2023;64(5):30. https://doi.org/10.1167/iovs.64.5.30

Purpose. To determine if the optic nerve head (ONH) response to transient elevated intraocular pressure (IOP) can predict the extent of neural loss in the nonhuman primate experimental glaucoma model.

Methods. The anterior chamber pressure of 21 healthy animals (5.4 ± 1.2 years, 8 female) was adjusted to 25 mm Hg for two hours followed by 10 mm Hg for an additional two hours. For the duration of IOP challenge the ONH was imaged using radial optical coherence tomography (OCT) scans at five-minute intervals. Afterward, a randomized sample of 14 of these subjects had unilateral experimental glaucoma induced and were monitored with OCT imaging, tonometry, and ocular biometry at two-week intervals.

Results. With pressure challenge, the maximum decrease in ONH minimum rim width (MRW) was 40 ± 10.5 µm at 25 mm Hg and was correlated with the precannulation MRW, Bruch's membrane opening (BMO) position, and the anterior lamina cribrosa surface position ($P = 0.01$). The maximum return of MRW at 10 mm Hg was 16.1 ± 5.0 µm and was not associated with any precannulation ONH feature ($P = 0.24$). However, healthy eyes with greater thickness return at 10 mm Hg had greater loss of MRW and retinal nerve fiber layer (RNFL) at a cumulative IOP of 1000 mm Hg · days after induction of experimental glaucoma. In addition, MRW and RNFL thinning was correlated with an increase in axial length ($P < 0.01$).

Conclusion. This study's findings suggest that the ONH's response to transient changes in IOP are associated with features of the ONH and surrounding tissues. The neural rim properties at baseline and the extent of axial elongation are associated with the severity of glaucomatous loss in the nonhuman primate model.

Keywords: experimental glaucoma, neuroretinal rim, axial length, optical coherence tomography

Primary open-angle glaucoma is a progressive optic neuropathy that results in irreversible vision loss. The exact mechanisms resulting in retinal ganglion cell loss remain elusive. Still, risk factors, including elevated intraocular pressure (IOP), age, race, central corneal thickness (CCT), axial elongation, and vertical cup-to-disc ratio, have been identified.[1–4] Management of glaucoma is limited to IOP reduction, which benefits patients with high- and normal-tension disease.[5–7] However, eyes with similar IOP profiles often have different progression rates.

Structural imaging with optical coherence tomography (OCT) is important for diagnosing and monitoring glaucoma. This includes measures of the circumpapillary retinal nerve fiber layer (RNFL) thickness, macula ganglion cell/inner plexiform layer thickness, and morphological measures of the optic nerve head (ONH), including the neuroretinal rim (NRR).[8,9] In principle, because measures of the RNFL, ganglion cell/inner plexiform layer, and NRR, all include elements of retinal ganglion cells (RGCs), they should have excellent correspondence. However, studies in human patients and animal models of glaucoma show that NRR thinning precedes that of the RNFL, suggesting that RGC insult may occur as axons are compressed or stretched at the rim margin.[10–12]

The ONH is considered a weak point, and several in vivo and histological studies have been undertaken to determine the response of the ONH and surrounding tissues to acute alterations in IOP. Initial studies in the nonhuman primate (NHP) identified the ONH lamina as a site for disruption of axon transport.[13–15] Furthermore, ex vivo and histological studies in control and experimental glaucoma eyes demonstrated alterations of the ONH and peripapillary tissue at fixed IOPs.[16–22] Some of these experiments were later repeated in vivo with anterior chamber cannulation, showing similar changes, albeit with lower resolution.[23–27] Such studies have identified the lamina and peripapillary connective tissue as important load-bearing structures susceptible to IOP stress.[28–31]

Using similar IOP challenge paradigms, we showed that the NRR, quantified as the minimum rim width (MRW), thins over a period of two hours at mild (25 mm Hg) and moderate (40 mm Hg) pressure settings.[32] Subsequently,

after this exposure, when IOP is set at 10 mm Hg, the NRR does not return to baseline over the same two hour period. Although animals showed similar trends, there was significant interindividual variability in tissue thinning and return, with pressure challenge. Furthermore, these changes were determined to be transient, because ONH metrics were similar to precannulation at follow-up OCT scanning sessions. We hypothesize that the extent of ONH NRR response to transient IOP modulation at baseline is related to early disease progression in the nonhuman primate experimental glaucoma model.

In healthy adult NHPs, transient IOP modulation can result in up to 60 µm of axial length change, which is not attributed to choroid thickness.[32] Chronic elevation of IOP in NHP experimental glaucoma is known to cause active remodeling of connective tissues,[28,33–40] whose property changes can be readily quantified with IOP modulation and ONH compliance.[23] In addition to ONH structure, we hypothesize that scleral remodeling with chronic pressure elevation also results in axial elongation, and the extent of elongation is associated with disease progression.

Methods

Subjects

A total of 21 rhesus monkeys (*Macaca mulatta*, eight females) ranging in age from 3.8 to 7.9 years (average age of 5.4 ± 1.2 years) were subjects for the first part of this study. Experimental glaucoma was induced in a random sample of 14 of these animals (average age 5.5 ± 1.1 years, five females). Randomization of subjects was done before any experimental intervention. For each subject, experimental interventions were performed only on one of the eyes. Experimental procedures and animal care protocols were approved by the Institutional Animal Care and Use Committee at the University of Houston. The use of animals for these experiments adhered to the ARVO Statement for the Use of Animals in Ophthalmic and Vision Research and to the National Institutes of Health guidelines for the care and use of laboratory animals.

Animal Preparation

Before any experimental intervention or imaging session, animals were anesthetized with an intramuscular injection of ketamine (20–25 mg/kg/h) and xylazine (0.8–0.9 mg/kg/h). Animals were also treated with a subcutaneous injection of atropine sulfate (0.04 mg/kg) to minimize salivation and maintain a healthy heart rate. While sedated, body temperature was maintained using a warm water blanket (Adroit Heat Therapy Pump and Pad; Adroit Medical, Loudon, TN, USA), and heart rate and blood oxygen saturation were monitored continuously (perMAP + II; Ramsey Medical, Tampa, FL, USA). Other than for trabecular meshwork laser sessions, the pupils were dilated with 1% tropicamide. At the end of each experiment, the effect of xylazine was reversed with atipamezole (0.06 mg/kg), and animals were monitored until they could be safely placed back in their home cage.

Anterior Chamber Cannulation and Pressure Control

All animals were subjects for a pressure challenge experiment with mild IOP increase. Animals were prepared as previously described.[32,41,42] In brief, after animals were sedated, 5% ophthalmic betadine (Alcon Laboratories, Fort Worth, TX, USA) was instilled on the ocular surface and used for cleaning the eyelids. After two minutes of exposure, the betadine was rinsed away with sterile balanced salt solution (Alcon Laboratories). The animal's head was stabilized, and a heat-sterilized speculum was used to hold the eyelids open.

The anterior chamber was cannulated using a sterile 27G butterfly needle, entering close to the limbus, with at least 1.5 mm of the needle visible in the anterior chamber. The needle was connected to a pressure control system consisting of a pressure transducer (Keller PR-41X; Keller America, Newport News, VA, USA) and syringe pump (Cole-Parmer, Vernon Hills, IL, USA) controlled with a custom program written in MATLAB (Mathworks, Natick, MA, USA). After needle insertion, a plano-powered rigid contact lens was placed on the cornea to maintain optical clarity.

For at least the first 15 minutes, anterior chamber pressure was maintained at 10 mm Hg, and several OCT scans were acquired to ensure good optical alignment and quality. Afterward, pressure was increased to 25 mm Hg for two hours. This pressure setting was selected because it is the approximate mean IOP of eyes with experimental glaucoma.[10] The duration of two hours was determined, because it is expected to capture 97% of the maximum MRW change, based on the average half-life from our previous studies.[32] OCT scans were acquired for the duration and at approximately five-minute intervals. After the last scan at 25 mm Hg, the pressure was reduced to 10 mm Hg, and scanning resumed for an additional two hours. At the end of the scanning session, the contact lens and needle were carefully removed, and a drop of broad-spectrum antibiotic was instilled on the ocular surface (polymyxin B/trimethoprim). To ensure animal health was maintained, sedation was limited to five hours, with experiments nominally starting at 7 AM so that animals could be recovered and returned for midafternoon feeding.

Laser Induced Ocular Hypertension

Fourteen (five female) of the 21 animals were randomized to have experimental glaucoma induced by scarring the trabecular meshwork using a 532 nm diode laser (Zeiss Visulas 532; Carl Zeiss Meditec, Jena, Germany). Contiguous laser applications were applied to the trabecular meshwork (TM) through a Kaufman single mirror gonioscopy lens (Ocular Instruments, Bellevue, WA, USA), with nominal power of 800 to 1000 mW, 50 µm spot size, and 500 msec duration. Laser power was adjusted to an ideal blanching of the TM tissue, minimizing "popping" and bleeding. The initial procedure involved lasering 180° of the angle, followed by 90° treatments at two- to three-week intervals until sustained elevated IOP was achieved. For all animals, one clock hour of the TM was left not lasered in an attempt to avoid excessive elevations in IOP. IOP was monitored using a Tono-Pen XL (Reichert, Inc., Depew, NY, USA) at each imaging session, typically every two weeks after the first laser procedure. Because xylazine can have IOP-lowering effects,[43] pressure measurements were made within five minutes of the animal entering the laboratory. The extent of IOP insult was calculated as cumulative IOP (mm Hg · days) using the IOP difference between the two eyes, referenced to the first laser session.[19,44]

Investigative Ophthalmology & Visual Science

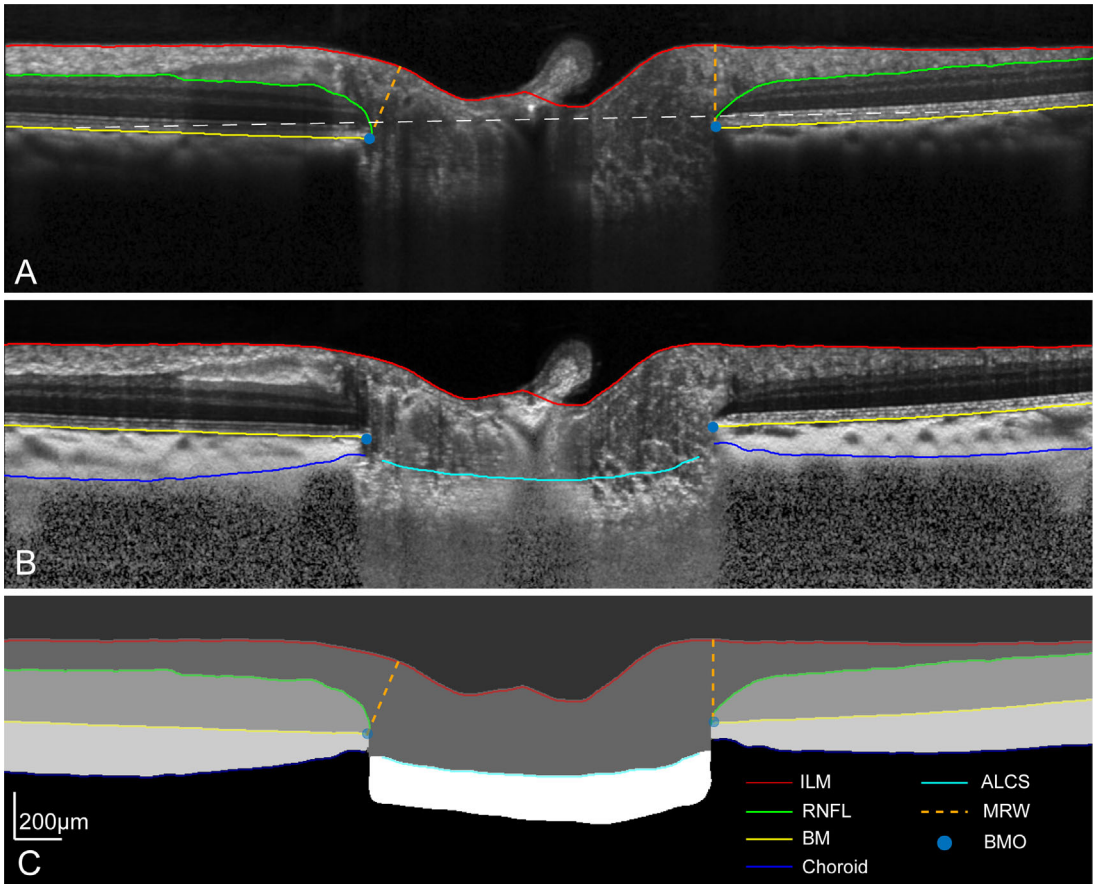

Figure 1. (**A**) A single OCT radial b-scan through the center of the optic nerve head, with segmentation for the ILM, RNFL, and BM. The *white dashed line* illustrates the 4 mm reference plane used to quantify BMO height. (**B**) B-scan compensated for light attenuation with choroid and ALCS segmentation.[48] (**C**) Semantic segmentation output from the neural network, illustrating all segmentation extracted.

Optical Coherence Tomography Imaging

Precannulation Imaging. Approximately two weeks before the cannulation experiment, baseline ocular biometry (Lenstar LS900; Haag-Streit, Koeniz, Switzerland) and OCT scans (Spectralis; Heidelberg Engineering, Heidelberg, Germany, central wavelength = 870 nm) were acquired for each subject. Data from these scans are referred to as the precannulation measures in the results and discussion. From optical biometry, CCT, anterior chamber depth, and axial length (AL) were used for data analysis. Although several OCT scans were obtained, the imaging used for this experiment included a 24-line 20° × 20° radial scan and a 193-line 20° × 20° raster scan centered on the ONH. Scans were captured using the high-resolution setting, in standard (non-EDI) mode, with at least nine frame averaging, and the autorescan feature was used for all follow-up imaging. For scan sessions in which animals had eye movements requiring repositioning of the scanning optics during a single scan acquisition, the radial scan was decreased to 12 lines and the raster scan to 97 lines. Scans were reacquired if quality fell below 30 dB. Analysis of these scans is described in the following sections.

Cannulation Imaging. For the duration of the cannulated experiments, radial scans were acquired at approximately five-minute intervals. To minimize variability from scan placement, images were obtained using the autorescan feature, using the precannulation scan as a baseline. After the experiment, scans were exported as "*.vol" files and analyzed using custom programs in Matlab, which incorporated individualized transverse scaling computed using a three-surface schematic eye.[45] To minimize bias, b-scans were segmented using a neural network trained on a DeepLabv3+ network based on ResNet-50.[46,47] This network was trained using 3731 manually segmented b-scans, which were compensated for light attenuation,[48] to an accuracy of 98.8% and loss of 0.03. The output segmentation from the neural networks was inspected for errors, corrected as needed, and analyzed as previously described (Fig. 1).[32,41] In brief, the Bruch's membrane opening (BMO) area was calculated from an ellipse fit to all the BMO points. The minimum distance from each BMO location to the inner limiting membrane (ILM) was used to compute the MRW. BMO height,[32,41] referred to as the BMO position in this work, was calculated as the perpendicular distance of the BMO to a 4 mm reference plane aligned to the Bruch's membrane and centered on the BMO. Using the BMO as a reference, the anterior lamina cribrosa surface (ALCS) position, for each b-scan, was determined for the central 50% of the lamina. For these two-dimensional analyses, data from each b-scan was weighted equally toward determining the average BMO and ALCS positions. Although the choroid and lamina thickness

Investigative Ophthalmology & Visual Science

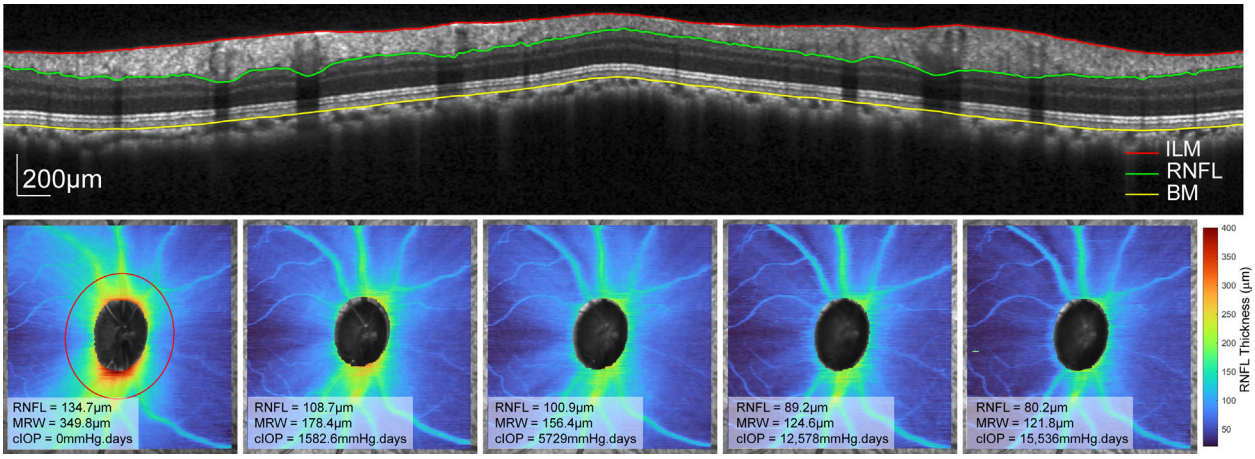

Figure 2. **Top row:** Circumpapillary b-scan, interpolated 550 µm from the BMO, with segmentation of the ILM, RNFL, and BM. **The bottom row** illustrates the RNFL thickness for the 20 × 20° scan region for a single subject across time. *The left panel* illustrates the 550 µm scan path (*red*), and each panel includes the circumpapillary RNFL thickness, MRW, and cumulative IOP.

were also extracted, these metrics have significant variability because of the limited visibility of deeper structures and were not used for analysis.

Longitudinal Imaging for Experimental Glaucoma. Fourteen of the 21 animals had laser-induced experimental glaucoma. Before the first laser session, each subject had at least four 20° × 20° baseline raster scans centered on the ONH. Afterward, animals nominally had repeat scans at two-week intervals. If IOP was greater than 25 mm Hg at any imaging session, a drop of dorzolamide 2%/timolol 0.5% was instilled to minimize the compressive effects of IOP on the ONH structures. Furthermore, experimental glaucoma eyes were scanned after the control eyes, approximately 40 minutes after IOP-lowering drop instillation. Raster scans were exported as "*.vol" files and segmented using a neural network trained on a DeepLabv3+ network based on ResNet-50.[46,47] This network was trained on 2761 manually segmented b-scans to an accuracy of 99.3% and loss of 0.01.[49] The output included segmentation of the ILM, RNFL, BM, and the BMO, which was interpolated across the scanned region. Before extracting thickness data, each scan and associated segmentation were rescaled to a 1:1 aspect ratio, incorporating individualized transverse scaling calculated using a three-surface schematic eye.[45] Using the BMO as a reference, the MRW was computed as the shortest distance to the ILM. Circumpapillary RNFL thickness was extracted from an interpolated scan path 550 µm from the BMO (Fig. 2, top).[45] Both the MRW and RNFL were used to assess disease progression (Fig. 2, bottom row), because these measures are related to total retrobulbar RGC axonal counts.[50,51]

Statistical Analysis

Data for the transient pressure challenge experiments were fit using Graphpad (GraphPad 9, Graphpad Software, SanDiego, CA), and as previously described (Fig. 3).[32] In brief, the 25 mm Hg portion of the data was fit with an exponential decay function (Equation 1), and the subsequent 10 mm Hg portion fit with an exponential rise to maximum function (Equation 2). The half-life for each of the two functions was calculated from the time constant (k), as ln (2)/k. From the exponential decay function, the difference between the y-intercept (y0) and plateau was used to determine the maximum predicted change at 25 mm Hg. Similarly, the y-intercept (y0) and plateau were used to calculate the tissue return for the 10 mm Hg segment. The difference between the initial measure of MRW (y0 for the exponential decay function), and the maximum tissue return (plateau) for the exponential rise function, was used to calculate the residual MRW thinning.

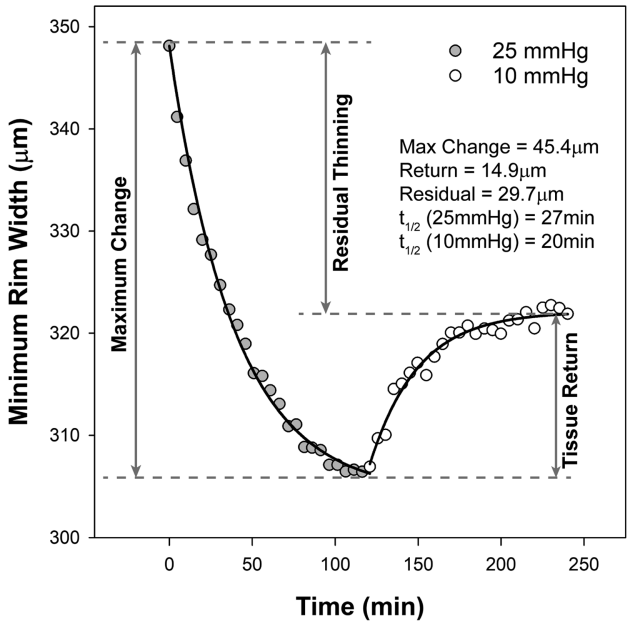

Figure 3. Data from one subject showing decrease in minimum rim with when pressure was set at 25 mm Hg (*gray symbols*), and tissue return with subsequent pressure at 10 mm Hg (*open symbols*). The plot illustrates how maximum change, tissue return and residual thinning were determined. Half-lives ($t_{1/2}$) were calculated using the time constant of each pressure segment.

$$\text{Exponential decay}: y = \text{plateau} + (y0 - \text{plateau}) \times e^{-k.\text{time}} \quad (1)$$

$$\text{Exponential rise}: y = y0 + (\text{plateau} - y0) \times (1 - e^{-k.\text{time}}) \quad (2)$$

The response of the optic nerve head and surrounding tissues to pressure modulation is complex, with significant interactions between structures. For this reason, stepwise regression analyses were performed to determine the correlation between the optic nerve head response to pressure challenge and baseline biometry measures and optic nerve head morphology. Regressions were performed for each pressure challenge metric as an outcome variable, including the maximum predicted change at 25 mm Hg, the maximum tissue return, and the time constants for both pressure segments. Predictor variables investigated included the baseline age, AL, CCT, and precannulation OCT measures of MRW, RNFL, BMO position, BMO area, and ACLS position. Predictor values with a probability less than 0.05 were included in the final model, and adjusted coefficient of determinations are reported. For analysis with significant relationships, the partial correlation for each predictor variable is included in the Supplementary Data. These analyses were performed using SPSS (Version 27.0; IBM Corp, Armonk, NY, USA).

The 14 animals with experimental glaucoma were also subjects for other studies and were monitored for extended durations (Fig. 7). In this experimental model, chronic elevated IOP is known to result in remodeling of ONH tissues.[19,28,38,52,53] To minimize the confounder of continuous connective tissue remodeling, early glaucoma was defined as the time when cumulative IOP reached 1000 mm Hg · days, and axial elongation was approaching an asymptote (see following discussion on axial elongation). Stepwise regression analysis was used to determine the correlation between individual metrics from the pre-glaucoma pressure challenge experiment, age of the animal, precannulation biometry, IOP, and the loss of MRW and circumpapillary RNFL at 1000 mm Hg · days. A separate analysis was performed to determine the relationship between changes in ocular biometry and loss of MRW and circumpapillary RNFL.

Results

Precannulation Baseline

At the baseline, precannulation imaging session, the average axial length of female animals was shorter (18.6 ± 0.6 mm) than males (19.1 ± 0.5 mm, $P = 0.04$, Table 1), but none of the OCT measures were related to axial length or sex ($P > 0.08$). Because there were no sex differences in ONH morphology, data from male and female animals are reported combined. The mean MRW was 335.1 ± 40.2 µm, and 129.9 ± 8.8 µm for circumpapillary RNFL thickness. The average BMO area was 1.41 ± 0.3 mm^2, with a BMO position of −28.5 ± 8.9 µm, and an ALCS position of −223.2 ± 63.8 µm.

Table 1. Comparison of Male and Female Measures of Axial Length and Baseline OCT Metrics

	Male (n = 13)	Female (n = 8)	*P*
Axial length (mm)	19.1 ± 0.5	18.6 ± 0.6	0.04
RNFL (µm)	132.5 ± 9.2	125.9 ± 6.8	0.08
MRW (µm)	341.9 ± 45.4	324.1 ± 29.2	0.29
BMO Area (mm^2)	1.42 ± 0.3	1.41 ± 0.4	0.97
BMO Position (µm)	−28.9 ± 7.2	−27.9 ± 11.9	0.83
ALCS Position (µm)	−221.8 ± 79.1	−225.5 ± 29.8	0.88

Pressure Challenge

The 21 animals maintained good systemic health for the study duration, with no complications noted after cannulation. For the duration of transient alteration in IOP, ONH morphology was assessed using radial scans acquired approximately every five minutes. The average signal strength of the b-scans was 37.1 ± 4.7 dB, and none of the images collected were removed from analysis because of misalignment or image quality. The anterior lamina surface for one animal was poorly delineated by the neural network and was manually corrected.

The predicted maximum changes and half-lives for the MRW were determined from the best fits with exponential functions (Equations 1 and 2). There were no differences in the maximum reduction of the MRW, maximum return, or the time constants between male and female subjects ($p > 0.26$), and the results presented are combined. The half-lives for the two pressure segments were similar (at 25 mm Hg, 22.5 ± 5.2 minutes, and at 10 mm Hg, 23.7 ± 15 minutes, $P = 0.74$) and suggest that the two-hour pressure exposure segments capture an accurate estimate of the maximum transient change with pressure challenge. Figure 4 illustrates the change in MRW for all 21 animals, referenced to the 10 mm Hg starting point before an IOP increase to 25 mm Hg (Figs. 4A, 4B). For better visualization of the variability in NRR return, data in Figure 4C are referenced to the two measures at 25 mm Hg before setting IOP to 10 mm Hg.

At an anterior chamber pressure of 25 mm Hg, each ONH showed thinning of the MRW, with a predicted maximum decrease of 40 ± 10.5 µm. A stepwise multiple regression analysis was used to determine if precannulation ONH metrics, ocular biometry or age, were associated with the extent of thinning. This analysis suggested that the maximum reduction in MRW could be predicted from the precannulation BMO position, MRW, and ALCS position (Maximum change in MRW = 11.5–0.67 BMO position + 0.1 MRW + 0.06 ALCS Depth, $R^2 = 0.56$, $P < 0.01$, Supplementary Table S1). The time constant for this segment was correlated to only the precannulation MRW (25 mm Hg time constant = −1.7 + 0.07 MRW, $R^2 = 0.27$, $P = 0.01$, Supplementary Table S2). For the 10 mm Hg segment, the predicted maximum return was 16.1 ± 5.0 µm, significantly less than the magnitude of decrease observed with 25 mm Hg ($P < 0.01$). In contrast to the 25 mm Hg segment, the maximum return of tissue, and the corresponding time constant was not related to any of the precannulation ONH metrics, ocular biometry or age ($P > 0.06$). Because the precannulation MRW was related to the maximum change at 25 mm Hg but not the tissue return for the 10 mm Hg segment, the residual thinning was expected to be linearly related to the maximum predicted change for the 25 mm Hg segment (Residual MRW = −15.2 + 0.94 MRW maximum change, $R^2 = 0.76$, $P < 0.01$).

When IOP was set at 25 mm Hg, there was no change in the BMO area (average change 0.002 ± 0.01 mm^2, $P = 0.57$). However, the BMO position moved posteriorly (mean change of 16.8 ± 11.1 µm), rapidly returning when the pressure was set to 10 mm Hg (mean difference = −0.9 ± 7.6 µm, $P = 0.6$, Fig. 5A). Using step-

Investigative Ophthalmology & Visual Science

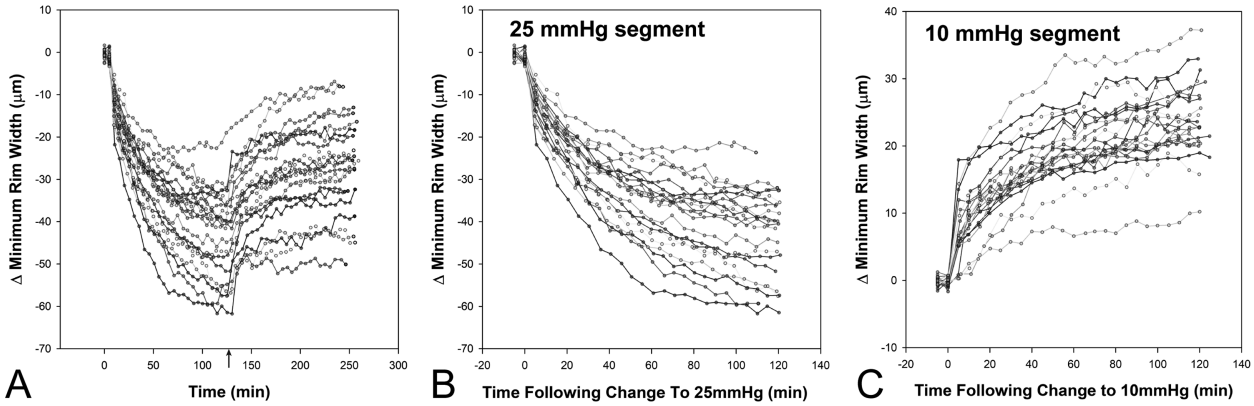

Figure 4. (**A**) Change in MRW referenced to measures before an increase to 25 mm Hg. (**B**) Isolated 25 mm Hg segment. (**C**) Isolated 10 mm Hg segment, with change referenced to the last two scans acquired at 25 mm Hg.

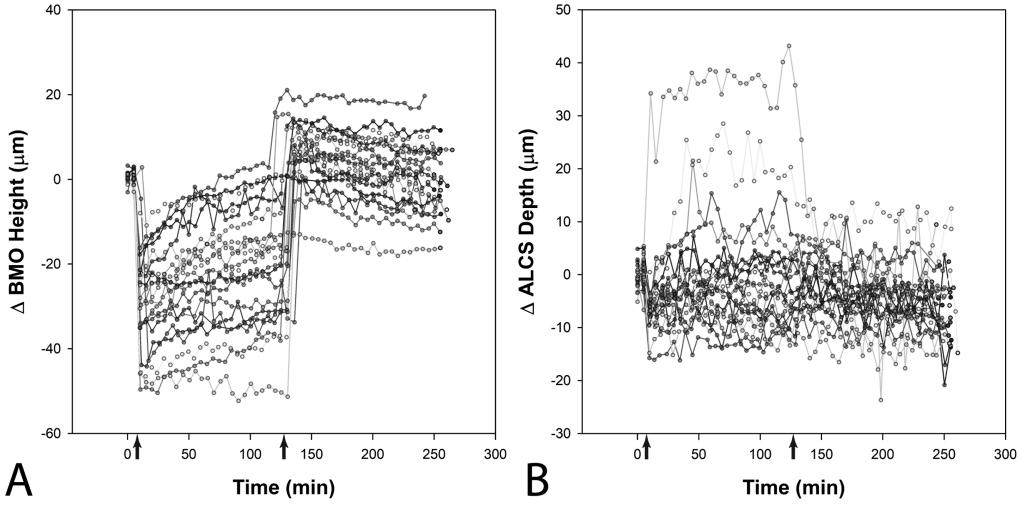

Figure 5. Change in BMO height (**A**) and ALCS depth (**B**) referenced to measures before an increase to 25 mm Hg. The *arrows* indicate the time at which pressure was changed to 25 mm Hg and then 10 mm Hg.

wise multiple regression analysis, the change in BMO position when IOP was raised to 25 mm Hg was correlated with the precannulation ALCS depth (Change in BMO position = 37.5 − 0.1 ALCS Depth, R^2 = 0.26, P = 0.01, Supplementary Table S3).

The ALCS position referenced to the BMO, moved posterior in 16 animals and anterior in five, at the 25 mm Hg pressure setting, returning to baseline at 10 mm Hg (P = 0.45). Of the five animals with an anterior ALCS movement, one was an outlier exceeding 30 μm (Fig. 5B). Although there was variability in ALCS response, stepwise multiple regression analysis suggested a relationship with precannulation measures of the MRW, BMO Area, ALCS position, and CCT (Change in ALCS position = −134.7 + 0.1 ALCS position + 0.1 MRW + 0.2 CCT − 8.0 BMO area, R^2 = 0.79, P < 0.01, Supplementary Table S4).

Glaucoma Progression

Fourteen of the 21 animals underwent laser scarring of the trabecular meshwork and were monitored with OCT at approximately two-week intervals to varying endpoints which were based on other unrelated studies. Table 2 compares the baseline characteristics of the experimental glaucoma sub-group to all animals used for the cannulation study. In this high-pressure experimental glaucoma model, as the cumulative IOP increases, there is a progressive loss of the ONH MRW and circumpapillary RNFL (Figs. 6A, 6B). The relationship between MRW and circumpapillary RNFL was best described by an exponential rise to maximum fit (R^2 = 0.80, Difference in AICc, compared to a linear fit = 59.4, Fig. 7C). This relationship was similar to that reported previously for a separate cohort of animals, suggesting a reduction of MRW before thinning of the RNFL.[10]

At every imaging session, axial length was measured using ocular biometry. Before the first trabecular meshwork lasering session, the two eyes had similar axial lengths (mean difference = 0.07 mm, P = 0.47); one animal was identified as an outlier with an axial length difference between the two eyes of 1.2 mm. The change in axial length with cumulative IOP was determined using the difference between the two eyes (Fig. 7). For this study, early disease was defined as the time point when change in axial length had stabilized. To determine this, the collective data of axial

Investigative Ophthalmology & Visual Science

Table 2. Comparison of Baseline Characteristics of the Experimental Glaucoma Subjects to the Entire Group

	Pressure Challenge Subjects (n = 21)	Experimental Glaucoma Subjects (n = 14)	*P*
Age (yrs)	5.4 ± 1.2	5.5 ± 1.1	0.82
Axial length (mm)	18.9 ± 0.6	18.9 ± 0.7	0.88
MRW (µm)	335.1 ± 40.1	333.7 ± 47.7	0.93
RNFL (µm)	130.0 ± 8.8	131.6 ± 10.1	0.64
BMO position (µm)	28.5 ± 8.9	29.8 ± 8.9	0.69
BMO area (mm^2)	1.42 ± 0.3	1.46 ± 0.4	0.76
ALCS position (µm)	223.2 ± 63.8	242.8 ± 63.5	0.38
Maximum change at 25 mm Hg (µm)	40.3 ± 10.5	40.4 ± 12.3	0.99
Maximum return at 10 mm Hg (µm)	16.1 ± 5.0	16.3 ± 4.9	0.90

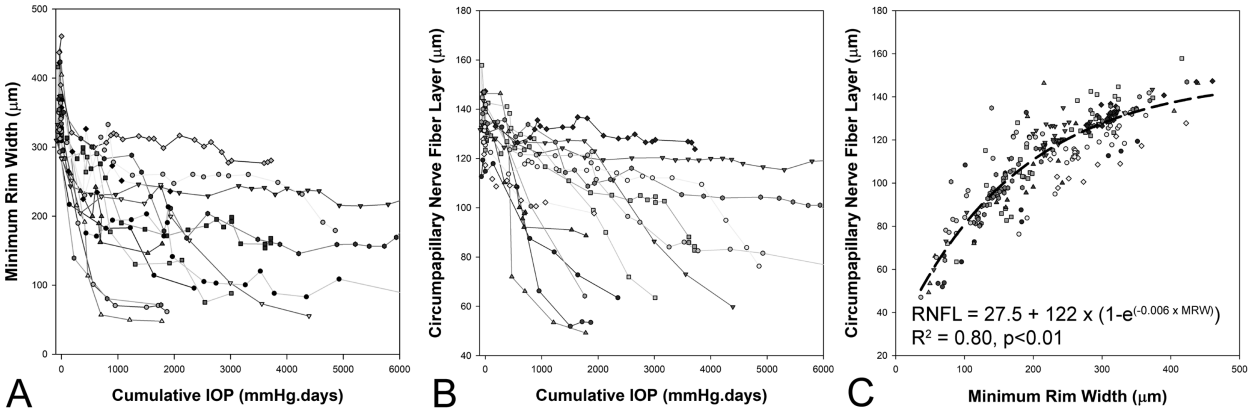

Figure 6. With increase in cumulative IOP, there is a reduction in MRW (**A**) and circumpapillary RNFL (**B**). The relationship between MRW and RNFL is best described using an exponential rise to maximum fit (**C**).

length and cumulative IOP from all subjects was fit with an exponential rise to maximum function. Based on this fit, the half-life was determined to be 256.7 mm Hg · days, suggesting that ~93% of the maximum axial length change had occurred by 1000 mm Hg · days. At this time point, the axial length of experimental glaucoma eyes had increased by up to 0.82 ± 0.53 mm ($P < 0.01$), was similar for both male and female animals ($P = 0.65$), and was not statistically different compared to endpoint (mean difference = 0.25 ± 0.39 mm, $P = 0.08$). The increase in axial length was mostly attributed to the vitreous chamber (Table 3), which we believe reflects the stress and strain on the sclera and associated remodeling with elevated IOP.[34,54] Hence, 1000 mm Hg · days was selected as the cutoff for analysis because later time points might not provide a meaningful comparison to baseline pressure challenge data. On average, the 1000 mm Hg · days timepoint was reached at 99.4 ± 28 days, and the imaging session closest to this date was used for determining change in MRW and circumpapillary RNFL thickness from the precannulation baseline. The average IOP after the last laser session up to this point was 25.5 ± 4.4 mm Hg, ranging from 19.6 to 35.3 mm Hg.

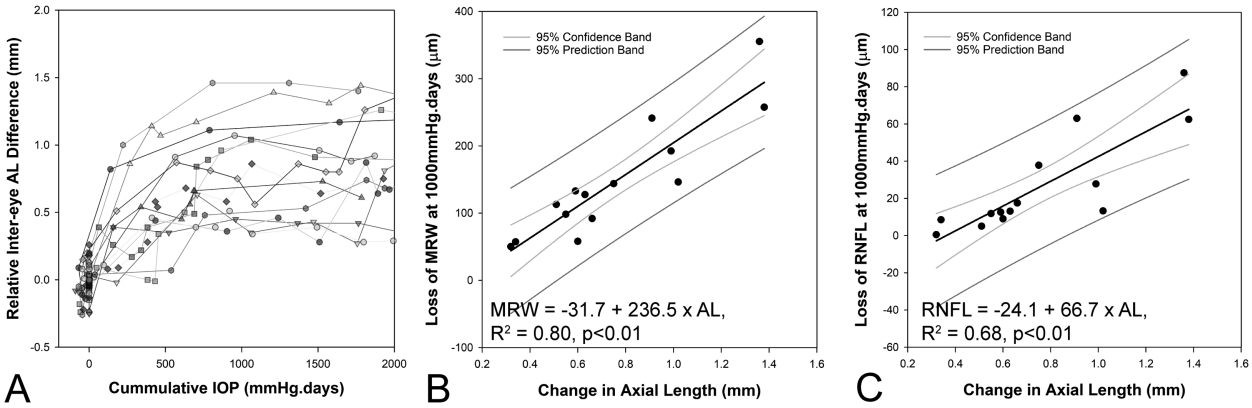

Figure 7. (**A**). Interocular difference in axial length increases with cumulative IOP up to 1000 mm Hg · days (data only shown to 2000 mm Hg · days, and relative to baseline intereye difference). Correlation between change in axial length and loss of MRW (**B**) and RNFL (**C**) At 1000 mm Hg · days.

Table 3. Intereye Differences (Experimental Glaucoma − Control Eye) in Ocular Biometry at Baseline, 1000 Mm Hg · Days, and at End Point

	Baseline	1000 mm Hg · Days	End Point	Repeated Measured ANOVA
Axial length	0.07 ± 0.34 mm	0.82 ± 0.53 mm	1.07 ± 0.45 mm	$P < 0.01$
Anterior chamber depth	−0.01 ± 0.07 mm	0.05 ± 0.10 mm	0.11 ± 0.26 mm	$P = 0.17$
Lens thickness	0.02 ± 0.05 mm	0.00 ± 0.08 mm	0.01 ± 0.10 mm	$P = 0.27$
Vitreous chamber depth	0.06 ± 0.33 mm	0.77 ± 0.53 mm	0.96 ± 0.39 mm	$P < 0.01$

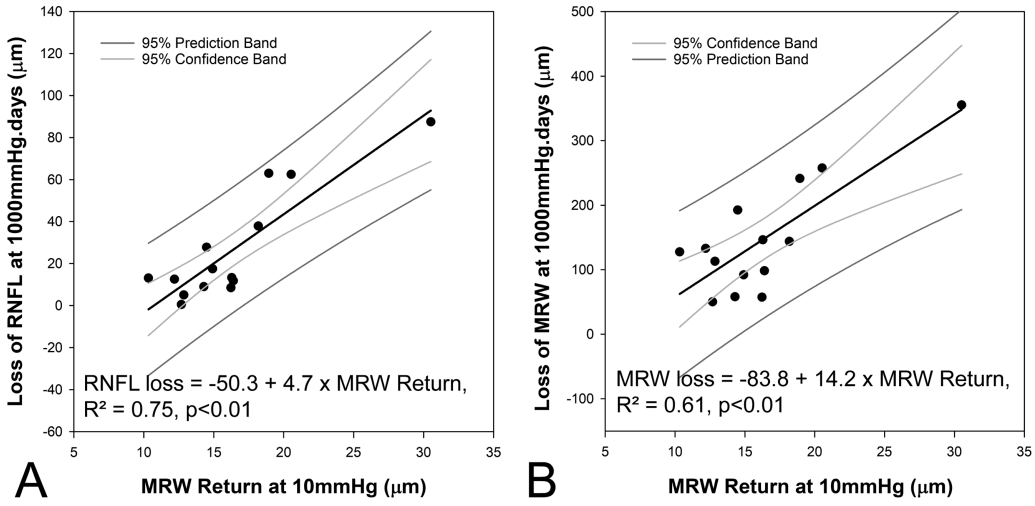

Figure 8. Relationship between loss of RNFL (**A**) and MRW (**B**) at 1000 mm Hg · days, and baseline pressure challenge measure of maximum MRW return at 10 mm Hg.

At 1000 mm Hg · days, the MRW was reduced by 147.5 ± 87.3 µm (range 51.3 to 355.3 µm) and the circumpapillary RNFL by 26.4 ± 26.4 µm (range 0.5 to 87.5 µm, Fig. 6) and was not significantly different between male and female animals ($P = 0.77$). In the stepwise regression, the reduction in MRW was related to the change in AL (Loss of MRW = $-31.7 + 236.4 \times$ change in AL, $R^2 = 0.80$, $P < 0.01$, Supplementary Table S5). For the loss of RNFL, in addition to the change in AL, baseline CCT was also identified as a significant predictor (Loss of RNFL = $-163.8 + 63.8 \times$ Change in AL $+ 0.30 \times$ CCT, $R^2 = 0.80$, $P < 0.01$, Supplementary Table S6). Figure 7 illustrates the change in axial length with cumulative IOP, and the association between the extent of axial elongation at 1000 mm Hg · days and the loss of MRW and RNFL (for illustration, CCT is not included).

A separate stepwise linear regression was performed to determine if the loss of MRW and RNFL at 1000 mm Hg · days were correlated with metrics from the pressure challenge experiments. This analysis identified the MRW return at 10 mm Hg as the only predictor variable for loss of both MRW and RNFL (Loss of MRW = $-83.8 + 14.2$ MRW return, $R^2 = 0.61$, $P < 0.01$, Loss of RNFL = $-50.3 + 4.7$ MRW return, $R^2 = 0.75$, $P < 0.01$; Figure 8, Supplementary Tables S7, S8).

Discussion

Glaucoma is a progressive optic neuropathy that has characteristic thinning of the ONH NRR tissue. Our previous studies showed that the NRR, quantified as the MRW, thins before the circumpapillary RNFL in NHP experimental glaucoma and that this relationship is present in a cross-sectional clinical cohort.[10] Furthermore, we demonstrated that, in healthy NHP eyes, the NRR response to an acute increase in anterior chamber pressure is prolonged over approximately two hours, and the NRR does not return to baseline over a similar time period.[32] The present work expands on these previous observations suggesting that the extent of NRR return following transient IOP increase can predict the susceptibility of RGCs in the nonhuman primate experimental glaucoma model. In addition, we show that at a specified cumulative IOP of 1000 mm Hg · days, the neural loss in our experimental subjects is correlated with axial elongation.

IOP is the only modifiable risk factor for glaucoma. Although IOP reduction is protective, individuals with similar pressure profiles can have significantly different outcomes. This likely reflects the complexity of the ONH region, which is often described as a biomechanical structure.[26,28,55,56] Under this framework, the peripapillary sclera and lamina are considered major load-bearing structures, and IOP-related stresses and strains on the neural and connective tissue can be substantial at all levels of IOP.[28] Further, these stresses and strains result in remodeling, which modifies the structural environment.[33,38–40,52,57] The present investigation was not designed to study the biomechanics of this region, but previous work in this area is instructive and is referenced in interpreting the findings. For clarity, discussion for the pressure challenge experiment in healthy eyes, and that for experimental glaucoma is presented separately.

Pressure Challenge Experiments in Healthy Eyes

Consistent with previous reports, the BMO area of healthy eyes, did not change with pressure modulation.[24,32,41,58]

However, when the anterior chamber pressure was set at 25 mm Hg, there was a posterior movement of the BMO, returning close to baseline when pressure was returned to 10 mm Hg. This change in BMO position at 25 mm Hg was negatively correlated with the precannulation ALCS position. In contrast to the BMO position, the response of the ALCS, when referenced to the BMO, is known to be highly variable with pressure modulation.[24,59–62] Although the present study showed similar variability, the stepwise regression suggested that the ALCS response can be predicted from the precannulation position of the lamina, precannulation MRW, precannulation BMO area and CCT. The inclusion of precannulation ALCS position in the model for both BMO and ALCS change with pressure challenge suggests that the extent of change is dependent on the connective tissue properties of the lamina. This is consistent with models that suggest that the normal-state ALCS and BMO positions may reflect peripapillary scleral compliance.[22,63–65]

In addition to precannulation ALCS position, the change in ALCS with pressure challenge, was correlated with the precannulation BMO area, precannulation MRW, and CCT. With pressure challenge, the scleral canal is known to expand, making the lamina taut.[22,64,66] The correlation of ALCS position change with BMO area suggests that anterior movement of the lamina expected with scleral expansion is possibly balanced by the posterior movement from perpendicular IOP forces related to the translaminar pressure difference. The inclusion of precannulation MRW in the model likely reflects the complex connective tissue framework surrounding axon bundles as they approach and pass through the lamina,[67] adding a structural element to how the lamina responds to a change in IOP. Histologically, in human eyes there is no association between CCT and central lamina thickness.[68,69] In contrast, the regression model suggests that lamina properties may have some association with CCT. Although the segmentation algorithm used in this study delineated the posterior surface of the lamina (Fig. 1), the visibility of this junction was variable, making lamina thickness an unreliable metric.

The circumpapillary RNFL response to transient IOP elevation was not quantified for the presented study. However, previous work in healthy NHP eyes has shown that transient modulation of IOP results in only minimal change in RNFL thickness compared to measures of the ONH NRR and prelaminar tissue.[24,25,41] We posit that differences in the adjacent regions may reflect regional anatomy. Although RGC axon bundles in the circumpapillary nerve fiber layer are surrounded by Müller glia, axon bundles in the rim tissue are guided by astrocytic channels.[67] In addition to the Müller glia and inner limiting membrane providing added tensile strength,[70,71] the fiber orientation in the two regions is different.[72] Both these factors could explain the significant differences in the magnitude of nerve fiber layer tissue change in these adjacent regions. Furthermore, these differences could contribute to the proposed hypothesis that axons are compressed, stretched, and possibly damaged at the rim margin.[11,67]

In our initial studies on the NRR response of healthy eyes to mild and moderate transient increases in IOP, none of the ONH response metrics were found to be associated with precannulation ONH features.[32] However, these studies were limited to data from eight subjects, which adequately described the prolonged change of the MRW but were not powered to determine the complex associations with baseline morphology. In this expanded study with 21 subjects, we limited the IOP challenge to a maximum of 25 mm Hg, because it corresponds to the average IOP in this experimental model. At this 25 mm Hg pressure, the maximum change of the MRW was found to be greatest in eyes with a larger precannulation MRW, smaller precannulation BMO positions and more posterior ALCS positions. Although the precannulation BMO and ALCS positions are not correlated, they possibly reflect the normal stresses and strains on the neural and connective tissues.

For the 10 mm Hg "recovery" segment of the pressure challenge experiments, the NRR increased but did not return to baseline in the two-hour observation period, consistent with previous studies.[32,41] However, at subsequent scan sessions, all ONH parameters had recovered to precannulation values, suggesting that the transient elevation of pressure did not have long-lasting effects on the ONH. In contrast to the 25 mm Hg segment, even with the expanded sample size, the recovery of the NRR at 10 mm Hg was not associated with any precannulation ONH metric. This suggests that the NRR tissue properties by itself is the primary determinant for 10 mm Hg segment increase in thickness.

Experimental Glaucoma

For the longitudinal study in subjects with experimental glaucoma, ONH metrics changed before circumpapillary RNFL thinning (Fig. 7C), which is consistent with previous reports using this model.[10,12,73–75] Based on the findings from the baseline cannulation experiments, it is probable that the early NRR changes are a reflection of elevated IOP and don't accurately represent a loss of RGC axons. To minimize the effects of high IOP on ONH structure, pressure-lowering drops were instilled in experimental eyes with high IOP at imaging sessions. Given that most imaging sessions lasted about an hour and the experimental eye was imaged second, the return of tissues, including the NRR, was expected to be stable at the time of imaging, assuming similar time constants to our pre-glaucoma cannulation experiments. However, from these pressure challenge experiments, the NRR tissue is known to have residual thinning, which cannot be accurately estimated (see Fig. 3). Similarly, we expect that with chronic pressure lowering, eyes with experimental glaucoma would have larger NRR measures at follow-up, as is seen in postsurgical glaucoma patients.[76–79]

Although there can be significant variability in IOP after lasering of the trabecular meshwork and induction of experimental glaucoma, the average IOP in the experimental group was similar to the pressure challenge setting of 25 mm Hg at baseline. For healthy NHP eyes, the MRW thinning using a pressure challenge of 25 mm Hg could be predicted from precannulation ONH metrics. However, the extent of MRW change including the associated time constant for the pre-glaucoma 25 mm Hg pressure segment was not related to the loss of MRW and RNFL at 1000 mm Hg · days after induction of experimental glaucoma. This is consistent with changes in ONH morphology and tissue remodeling with disease progression.[33,38–40,52,57] These findings also suggest that the connective tissue remodeling response cannot be predicted based on the structural measurements quantified in this study.

In contrast to the 25 mm Hg segment of the pressure challenge experiment, the MRW return at 10 mm Hg was not associated with any precannulation ONH metric. However, this MRW return, determined before induction of experimental glaucoma, was positively correlated with nerve fiber layer

loss at 1000 mm Hg · days. These findings would suggest that the tissue properties of the neural tissue alone are associated with the risk of axonal loss. These findings are clinically relevant as reversal of ONH morphology has also been reported following therapeutic intervention in patients with glaucoma.[76–84] However, the significance of these findings remains unknown. If validated by other studies, our findings would suggest that evaluating both acute and short-term changes of the NRR, to determine maximum return and residual NRR metrics, could contribute to disease progression risk assessment.

Connective tissue remodeling[39,40,57] with chronic elevated IOP has been demonstrated as hypercompliance of the lamina to pressure change in early disease,[17,26,85–87] changes in lamina thickness,[52] and by glaucomatous eyes having stiffer scleras.[34,54] We posit that remodeling of the sclera, in the current study, is reflected in axial elongation. Up to a cumulative pressure of 1000 mm Hg · days, experimental eyes lengthened but by varying degrees. Although there were modest changes in the anterior chamber depth, the majority of lengthening could be accounted for by the vitreous chamber. Furthermore, one of the major findings of this work is that eyes with greater axial elongation had more significant thinning of both the MRW and the RNFL. Connective tissue properties with remodeling are known to change with total pressure exposure, likely reflecting susceptibility to IOP.[88,89] It is also plausible that axial elongation stretches axons, making them more susceptible to damage.[90] We hypothesize that the combination of connective tissue remodeling and stretch on the axons are additive. Because each of the animals in this study was emmetropic before cannulation, it could not be determined whether eyes with significant refractive error would respond similarly. The findings on axial length could be clinically relevant because changes in eye length have been noted after IOP reduction[91–93]; however, their clinical relevance on disease progression is unknown.

Limitations

In the present study, age was not associated with any of the cannulated metrics or disease progression. Although subjects for this study were all mature adults, they were relatively young and with a narrow age range. Because the biomechanics of the optic nerve head and properties of the sclera are related to age,[31,94,95] it is likely that the correlations with the cannulated studies would reflect these if older animals were included in the study. Similarly, it is anticipated that the axial elongation observed with disease progression would be age dependent.

This study has several additional limitations. Although many of the correlations were significant, our sample size was relatively small. Although the pressure transducer used was calibrated, resistance of the tubing and needle were not accounted for. Hence, it is possible that there is a lag in pressure change when pressure is modulated. Because structural changes were observed over extended periods of time, we expect this effect would have minimal impact on the exponential fits. A strength of this work was the use of a neural network-based algorithm for image segmentation. Although this added objectivity, errors in segmentation had to be manually corrected, and several features including the scleral canal opening, lamina thickness, and three-dimensional shape of the BMO were not assessed. Furthermore, the BMO position should ideally be referenced to the choroid/sclera junction.[41,96] Although this junction was visible in most of our subjects, variability in pigmentation prevented the accurate identification of this junction for several animals. For the experimental glaucoma model, the IOP response to laser scarring of the trabecular meshwork can be highly variable. Although all attempts were made to minimize pressure spikes after lasering, these cannot be accounted for. Optimally, anterior chamber pressure would be monitored continuously,[97] and OCT-based structural measures would be acquired at more frequent intervals to better characterize IOP-associated structural changes. It is possible that a portion of the observed axial elongation could be a result of choroid thinning. Although sub-macula choroid thickness was not monitored, changes in peripapillary choroid thickness were not significantly reduced at 1000 mm Hg · days (-2.6 ± 14.6 µm, $P = 0.5$, Supplementary Fig. S1). Last, this study did not consider factors of vasculature or cerebrospinal fluid pressure,[98–101] both of which have been associated with glaucoma pathophysiology.

Conclusion

In conclusion, this study shows that the NRR response to transient pressure elevation in healthy NHP eyes is related to ONH features, including the peripapillary tissue. Although the NRR return in the cannulation experiment was not associated with any baseline ONH metric, eyes with a greater return at baseline had a more significant loss of MRW and RNFL at 1000 mm Hg · days of experimental glaucoma. Furthermore, the loss of MRW and RNFL in NHP experimental glaucoma, was related to the increase in axial length. These data support the idea that NRR properties, axonal stretch, and connective tissue remodeling are important factors in glaucoma progression.

Acknowledgments

Supported by NIH grants: P30 EY007551, R01 EY029229, and the UH Mary Murphy Endowment.

Disclosure: **N.B. Patel,** None; **L. Carter-Dawson,** None; **L.J. Frishman,** None

References

1. Heijl A, Leske MC, Bengtsson B, Hyman L, Bengtsson B, Hussein M. Reduction of intraocular pressure and glaucoma progression: results from the Early Manifest Glaucoma Trial. *Arch Ophthalmol*. 2002;120:1268–1279.
2. Miglior S, Pfeiffer N, Torri V, Zeyen T, Cunha-Vaz J, Adamsons I. Predictive factors for open-angle glaucoma among patients with ocular hypertension in the European Glaucoma Prevention Study. *Ophthalmology*. 2007;114:3–9.
3. Gordon MO, Beiser JA, Brandt JD, et al. The Ocular Hypertension Treatment Study: baseline factors that predict the onset of primary open-angle glaucoma. *Arch Ophthalmol*. 2002;120:714–720.
4. Mitchell P, Hourihan F, Sandbach J, Wang JJ. The relationship between glaucoma and myopia: the Blue Mountains Eye Study. *Ophthalmology*. 1999;106:2010–2015.
5. Leske MC, Hyman L, Hussein M, Heijl A, Bengtsson B. Comparison of glaucomatous progression between untreated patients with normal-tension glaucoma and patients with therapeutically reduced intraocular

pressures. The effectiveness of intraocular pressure reduction in the treatment of normal-tension glaucoma. *Am J Ophthalmol*. 1999;127:625–626.
6. The Advanced Glaucoma Intervention Study (AGIS): 7. The relationship between control of intraocular pressure and visual field deterioration. The AGIS Investigators. *Am J Ophthalmol*. 2000;130:429–440.
7. Anderson DR. Glaucoma: the damage caused by pressure. XLVI Edward Jackson memorial lecture. *Am J Ophthalmol*. 1989;108:485–495.
8. Leung CK. Diagnosing glaucoma progression with optical coherence tomography. *Curr Opin Ophthalmol*. 2014;25:104–111.
9. Bussel II, Wollstein G, Schuman JS. OCT for glaucoma diagnosis, screening and detection of glaucoma progression. *Br J Ophthalmol*. 2014;98(Suppl 2):ii15–ii19.
10. Patel NB, Sullivan-Mee M, Harwerth RS. The relationship between retinal nerve fiber layer thickness and optic nerve head neuroretinal rim tissue in glaucoma. *Invest Ophthalmol Vis Sci*. 2014;55:6802–6816.
11. Fortune B, Reynaud J, Hardin C, Wang L, Sigal IA, Burgoyne CF. Experimental glaucoma causes optic nerve head neural rim tissue compression: a potentially important mechanism of axon injury. *Invest Ophthalmol Vis Sci*. 2016;57:4403–4411.
12. He L, Yang H, Gardiner SK, et al. Longitudinal detection of optic nerve head changes by spectral domain optical coherence tomography in early experimental glaucoma. *Invest Ophthalmol Vis Sci*. 2014;55:574–586.
13. Anderson DR, Hendrickson A. Effect of intraocular pressure on rapid axoplasmic transport in monkey optic nerve. *Invest Ophthalmol*. 1974;13:771–783.
14. Quigley H, Anderson DR. The dynamics and location of axonal transport blockade by acute intraocular pressure elevation in primate optic nerve. *Invest Ophthalmol*. 1976;15:606–616.
15. Quigley HA, Anderson DR. Distribution of axonal transport blockade by acute intraocular pressure elevation in the primate optic nerve head. *Invest Ophthalmol Vis Sci*. 1977;16:640–644.
16. Levy NS, Crapps EE, Bonney RC. Displacement of the optic nerve head. Response to acute intraocular pressure elevation in primate eyes. *Arch Ophthalmol*. 1981;99:2166–2174.
17. Bellezza AJ, Rintalan CJ, Thompson HW, Downs JC, Hart RT, Burgoyne CF. Deformation of the lamina cribrosa and anterior scleral canal wall in early experimental glaucoma. *Invest Ophthalmol Vis Sci*. 2003;44:623–637.
18. Burgoyne CF, Downs JC, Bellezza AJ, Hart RT. Three-dimensional reconstruction of normal and early glaucoma monkey optic nerve head connective tissues. *Invest Ophthalmol Vis Sci*. 2004;45:4388–4399.
19. Yang H, Thompson H, Roberts MD, Sigal IA, Downs JC, Burgoyne CF. Deformation of the early glaucomatous monkey optic nerve head connective tissue after acute IOP elevation in 3-D histomorphometric reconstructions. *Invest Ophthalmol Vis Sci*. 2011;52:345–363.
20. Yang H, Williams G, Downs JC, et al. Posterior (outward) migration of the lamina cribrosa and early cupping in monkey experimental glaucoma. *Invest Ophthalmol Vis Sci*. 2011;52:7109–7121.
21. Fatehee N, Yu PK, Morgan WH, Cringle SJ, Yu DY. The impact of acutely elevated intraocular pressure on the porcine optic nerve head. *Invest Ophthalmol Vis Sci*. 2011;52:6192–6198.
22. Bellezza AJ, Rintalan CJ, Thompson HW, Downs JC, Hart RT, Burgoyne CF. Anterior scleral canal geometry in pressurised (IOP 10) and non-pressurised (IOP 0) normal monkey eyes. *Br J Ophthalmol*. 2003;87:1284–1290.
23. Ivers KM, Yang H, Gardiner SK, et al. In vivo detection of laminar and peripapillary scleral hypercompliance in early monkey experimental glaucoma. *Invest Ophthalmol Vis Sci*. 2016;57:Oct388–Oct403.
24. Strouthidis NG, Fortune B, Yang H, Sigal IA, Burgoyne CF. Effect of acute intraocular pressure elevation on the monkey optic nerve head as detected by spectral domain optical coherence tomography. *Invest Ophthalmol Vis Sci*. 2011;52:9431–9437.
25. Fortune B, Yang H, Strouthidis NG, et al. The effect of acute intraocular pressure elevation on peripapillary retinal thickness, retinal nerve fiber layer thickness, and retardance. *Invest Ophthalmol Vis Sci*. 2009;50:4719–4726.
26. Heickell AG, Bellezza AJ, Thompson HW, Burgoyne CF. Optic disc surface compliance testing using confocal scanning laser tomography in the normal monkey eye. *J Glaucoma*. 2001;10:369–382.
27. Quigley HA, Pease ME. Change in the optic disc and nerve fiber layer estimated with the glaucoma-scope in monkey eyes. *J Glaucoma*. 1996;5:106–116.
28. Burgoyne CF, Downs JC, Bellezza AJ, Suh JK, Hart RT. The optic nerve head as a biomechanical structure: a new paradigm for understanding the role of IOP-related stress and strain in the pathophysiology of glaucomatous optic nerve head damage. *Prog Retin Eye Res*. 2005;24:39–73.
29. Yang H, Reynaud J, Lockwood H, et al. The connective tissue phenotype of glaucomatous cupping in the monkey eye—clinical and research implications. *Prog Retin Eye Res*. 2017;59:1–52.
30. Burgoyne CF. A biomechanical paradigm for axonal insult within the optic nerve head in aging and glaucoma. *Exp Eye Res*. 2011;93:120–132.
31. Downs JC. Optic nerve head biomechanics in aging and disease. *Exp Eye Res*. 2015;133:19–29.
32. Pardon LP, Harwerth RS, Patel NB. Neuroretinal rim response to transient changes in intraocular pressure in healthy non-human primate eyes. *Exp Eye Res*. 2020;193:107978.
33. Downs JC, Suh JK, Thomas KA, Bellezza AJ, Hart RT, Burgoyne CF. Viscoelastic material properties of the peripapillary sclera in normal and early-glaucoma monkey eyes. *Invest Ophthalmol Vis Sci*. 2005;46:540–546.
34. Coudrillier B, Tian J, Alexander S, Myers KM, Quigley HA, Nguyen TD. Biomechanics of the human posterior sclera: age- and glaucoma-related changes measured using inflation testing. *Invest Ophthalmol Vis Sci*. 2012;53:1714–1728.
35. Myers KM, Cone FE, Quigley HA, Gelman S, Pease ME, Nguyen TD. The in vitro inflation response of mouse sclera. *Exp Eye Res*. 2010;91:866–875.
36. Girard MJ, Downs JC, Burgoyne CF, Suh JK. Peripapillary and posterior scleral mechanics—part I: development of an anisotropic hyperelastic constitutive model. *J Biomech Eng*. 2009;131:051011.
37. Girard MJ, Suh JK, Bottlang M, Burgoyne CF, Downs JC. Biomechanical changes in the sclera of monkey eyes exposed to chronic IOP elevations. *Invest Ophthalmol Vis Sci*. 2011;52:5656–5669.
38. Downs JC, Ensor ME, Bellezza AJ, Thompson HW, Hart RT, Burgoyne CF. Posterior scleral thickness in perfusion-fixed normal and early-glaucoma monkey eyes. *Invest Ophthalmol Vis Sci*. 2001;42:3202–3208.
39. Hernandez MR. The optic nerve head in glaucoma: role of astrocytes in tissue remodeling. *Prog Retin Eye Res*. 2000;19:297–321.
40. Hernandez MR, Pena JDO. The optic nerve head in glaucomatous optic neuropathy. *Arch Ophthalmol*. 1997;115:389–395.

Investigative Ophthalmology & Visual Science

41. Patel N, McAllister F, Pardon L, Harwerth R. The effects of graded intraocular pressure challenge on the optic nerve head. *Exp Eye Res*. 2018;169:79–90.
42. McAllister F, Harwerth R, Patel N. Assessing the true intraocular pressure in the non-human primate. *Optom Vis Sci*. 2018;95:113–119.
43. Frishman LJ, Shen FF, Du L, et al. The scotopic electroretinogram of macaque after retinal ganglion cell loss from experimental glaucoma. *Invest Ophthalmol Vis Sci*. 1996;37:125–141.
44. Harwerth RS, Smith EL, DeSantis L. Experimental glaucoma: perimetric field defects and intraocular pressure. *J Glaucoma*. 1997;6:390–401.
45. Patel NB, Luo X, Wheat JL, Harwerth RS. Retinal nerve fiber layer assessment: area versus thickness measurements from elliptical scans centered on the optic nerve. *Invest Ophthalmol Vis Sci*. 2011;52:2477–2489.
46. Chen L-C, Papandreou G, Schroff F, Adam H. Rethinking atrous convolution for semantic image segmentation. *arXiv preprint arXiv:170605587* 2017.
47. He K, Zhang X, Ren S, Sun J. Deep residual learning for image recognition. *Proc IEEE Conference on Comput Vis Pattern Recognit*. 2016:770–778.
48. Girard MJ, Strouthidis NG, Ethier CR, Mari JM. Shadow removal and contrast enhancement in optical coherence tomography images of the human optic nerve head. *Invest Ophthalmol Vis Sci*. 2011;52:7738–7748.
49. Srinivasan VV, Das S, Patel N. Widefield OCT imaging for quantifying inner retinal thickness in the nonhuman primate. *Transl Vis Sci Technol*. 2022;11:12.
50. Antwi-Boasiako K, Carter-Dawson L, Harwerth R, Gondo M, Patel N. The relationship between macula retinal ganglion cell density and visual function in the nonhuman primate. *Invest Ophthalmol Vis Sci*. 2021;62:5.
51. Cull GA, Reynaud J, Wang L, Cioffi GA, Burgoyne CF, Fortune B. Relationship between orbital optic nerve axon counts and retinal nerve fiber layer thickness measured by spectral domain optical coherence tomography. *Invest Ophthalmol Vis Sci*. 2012;53:7766–7773.
52. Roberts MD, Grau V, Grimm J, et al. Remodeling of the connective tissue microarchitecture of the lamina cribrosa in early experimental glaucoma. *Invest Ophthalmol Vis Sci*. 2009;50:681–690.
53. Crawford Downs J, Roberts MD, Sigal IA. Glaucomatous cupping of the lamina cribrosa: a review of the evidence for active progressive remodeling as a mechanism. *Exp Eye Res*. 2011;93:133–140.
54. Jia X, Zhang F, Cao M, et al. Elevated IOP Alters the Material Properties of Sclera and Lamina Cribrosa in Monkeys. *Dis Markers*. 2022;2022:5038847.
55. Zeimer RC, Ogura Y. The relation between glaucomatous damage and optic nerve head mechanical compliance. *Arch Ophthalmol*. 1989;107:1232–1234.
56. Campbell IC, Coudrillier B, Ross Ethier C. Biomechanics of the posterior eye: a critical role in health and disease. *J Biomech Eng*. 2014;136:021005.
57. Hernandez MR, Pena JD, Selvidge JA, Salvador-Silva M, Yang P. Hydrostatic pressure stimulates synthesis of elastin in cultured optic nerve head astrocytes. *Glia*. 2000;32:122–136.
58. Fazio MA, Johnstone JK, Smith B, Wang L, Girkin CA. Displacement of the lamina cribrosa in response to acute intraocular pressure elevation in normal individuals of African and European descent. *Invest Ophthalmol Vis Sci*. 2016;57:3331–3339.
59. Agoumi Y, Sharpe GP, Hutchison DM, Nicolela MT, Artes PH, Chauhan BC. Laminar and prelaminar tissue displacement during intraocular pressure elevation in glaucoma patients and healthy controls. *Ophthalmology*. 2011;118:52–59.
60. Yang H, Downs JC, Sigal IA, Roberts MD, Thompson H, Burgoyne CF. Deformation of the normal monkey optic nerve head connective tissue after acute IOP elevation within 3-D histomorphometric reconstructions. *Invest Ophthalmol Vis Sci*. 2009;50:5785–5799.
61. Quigley H, Arora K, Idrees S, et al. Biomechanical responses of lamina cribrosa to intraocular pressure change assessed by optical coherence tomography in glaucoma eyes. *Invest Ophthalmol Vis Sci*. 2017;58:2566–2577.
62. Tun TA, Thakku SG, Png O, et al. Shape changes of the anterior lamina cribrosa in normal, ocular hypertensive, and glaucomatous eyes following acute intraocular pressure elevation. *Invest Ophthalmol Vis Sci*. 2016;57:4869–4877.
63. Yang H, Reynaud J, Lockwood H, et al. The connective tissue phenotype of glaucomatous cupping in the monkey eye—clinical and research implications. *Progr Retinal Eye Res*. 2017;59:1–52.
64. Sigal IA, Yang H, Roberts MD, Burgoyne CF, Downs JC. IOP-induced lamina cribrosa displacement and scleral canal expansion: an analysis of factor interactions using parameterized eye-specific models. *Invest Ophthalmol Vis Sci*. 2011;52:1896–1907.
65. Sigal IA, Flanagan JG, Tertinegg I, Ethier CR. Predicted extension, compression and shearing of optic nerve head tissues. *Exp Eye Res*. 2007;85:312–322.
66. Ma Y, Pavlatos E, Clayson K, et al. Mechanical deformation of human optic nerve head and peripapillary tissue in response to acute IOP elevation. *Invest Ophthalmol Vis Sci*. 2019;60:913–920.
67. Oyama T, Abe H, Ushiki T. The connective tissue and glial framework in the optic nerve head of the normal human eye: light and scanning electron microscopic studies. *Arch Histol Cytol*. 2006;69:341–356.
68. Ren R, Li B, Gao F, et al. Central corneal thickness, lamina cribrosa and peripapillary scleral histomorphometry in non-glaucomatous Chinese eyes. *Graefes Arch Clin Exp Ophthalmol*. 2010;248:1579–1585.
69. Jonas JB, Holbach L. Central corneal thickness and thickness of the lamina cribrosa in human eyes. *Invest Ophthalmol Vis Sci*. 2005;46:1275–1279.
70. MacDonald RB, Randlett O, Oswald J, Yoshimatsu T, Franze K, Harris WA. Müller glia provide essential tensile strength to the developing retina. *J Cell Biol*. 2015;210:1075–1083.
71. Lundkvist A, Reichenbach A, Betsholtz C, Carmeliet P, Wolburg H, Pekny M. Under stress, the absence of intermediate filaments from Müller cells in the retina has structural and functional consequences. *J Cell Sci*. 2004;117:3481–3488.
72. Giordano C, Cloots RJ, van Dommelen JA, Kleiven S. The influence of anisotropy on brain injury prediction. *J Biomech*. 2014;47:1052–1059.
73. Strouthidis NG, Fortune B, Yang H, Sigal IA, Burgoyne CF. Longitudinal change detected by spectral domain optical coherence tomography in the optic nerve head and peripapillary retina in experimental glaucoma. *Invest Ophthalmol Vis Sci*. 2011;52:1206–1219.
74. Fortune B, Reynaud J, Wang L, Burgoyne CF. Does optic nerve head surface topography change prior to loss of retinal nerve fiber layer thickness: a test of the site of injury hypothesis in experimental glaucoma. *PLoS One*. 2013;8:e77831.
75. Ivers KM, Sredar N, Patel NB, et al. In vivo changes in lamina cribrosa microarchitecture and optic nerve

Investigative Ophthalmology & Visual Science

head structure in early experimental glaucoma. *PLoS One*. 2015;10:e0134223.
76. Gietzelt C, Lüke JN, Adler W, et al. Short-term changes in Bruch's membrane opening-based morphometrics during the first week after trabeculectomy. *Graefes Arch Clin Exp Ophthalmol*. 2022;260:3321–3329.
77. Lesk MR, Spaeth GL, Azuara-Blanco A, et al. Reversal of optic disc cupping after glaucoma surgery analyzed with a scanning laser tomograph. *Ophthalmology*. 1999;106:1013–1018.
78. Glaser TS, Go MS, Kelly MP, Dairi MA, Freedman SF. Intraoperative mounted optical coherence tomography findings following reversal of optic nerve head cupping in childhood glaucoma. *Am J Ophthalmol*. 2022;243:109–117.
79. Girard MJ, Beotra MR, Chin KS, et al. In vivo 3-dimensional strain mapping of the optic nerve head following intraocular pressure lowering by trabeculectomy. *Ophthalmology*. 2016;123:1190–1200.
80. Ely AL, El-Dairi MA, Freedman SF. Cupping reversal in pediatric glaucoma—evaluation of the retinal nerve fiber layer and visual field. *Am J Ophthalmol*. 2014;158:905–915.
81. Jiang R, Xu L, Liu X, Chen JD, Jonas JB, Wang YX. Optic nerve head changes after short-term intraocular pressure elevation in acute primary angle-closure suspects. *Ophthalmology*. 2015;122:730–737.
82. Raghu N, Pandav SS, Kaushik S, Ichhpujani P, Gupta A. Effect of trabeculectomy on RNFL thickness and optic disc parameters using optical coherence tomography. *Eye (Lond)*. 2012;26:1131–1137.
83. Barrancos C, Rebolleda G, Oblanca N, Cabarga C, Munoz-Negrete FJ. Changes in lamina cribrosa and prelaminar tissue after deep sclerectomy. *Eye (Lond)*. 2014;28:58–65.
84. Lee EJ, Kim TW, Weinreb RN. Reversal of lamina cribrosa displacement and thickness after trabeculectomy in glaucoma. *Ophthalmology*. 2012;119:1359–1366.
85. Ivers KM, Yang H, Gardiner SK, et al. In vivo detection of laminar and peripapillary scleral hypercompliance in early monkey experimental glaucoma. *Invest Ophthalmol Vis Sci*. 2016;57:OCT388–OCT403.
86. Burgoyne CF, Quigley HA, Thompson HW, Vitale S, Varma R. Early changes in optic disc compliance and surface position in experimental glaucoma. *Ophthalmology*. 1995;102:1800–1809.
87. Burgoyne CF, Quigley HA, Thompson HW, Vitale S, Varma R. Measurement of optic disc compliance by digitized image analysis in the normal monkey eye. *Ophthalmology*. 1995;102:1790–1799.
88. Fazio MA, Girard MJA, Lee W, Morris JS, Burgoyne CF, Downs JC. The relationship between scleral strain change and differential cumulative intraocular pressure exposure in the nonhuman primate chronic ocular hypertension model. *Invest Ophthalmol Vis Sci*. 2019;60:4141–4150.
89. Cone-Kimball E, Nguyen C, Oglesby EN, Pease ME, Steinhart MR, Quigley HA. Scleral structural alterations associated with chronic experimental intraocular pressure elevation in mice. *Mol Vis*. 2013;19:2023–2039.
90. Fortune B. Pulling and tugging on the retina: mechanical impact of glaucoma beyond the optic nerve head. *Invest Ophthalmol Vis Sci*. 2019;60:26–35.
91. Cashwell LF, Martin CA. Axial length decrease accompanying successful glaucoma filtration surgery. *Ophthalmology*. 1999;106:2307–2311.
92. Francis BA, Wang M, Lei H, et al. Changes in axial length following trabeculectomy and glaucoma drainage device surgery. *Br J Ophthalmol*. 2005;89:17–20.
93. Kim C-s, Kim KN, Kang TS, Jo YJ, Kim JY. Changes in axial length and refractive error after noninvasive normalization of intraocular pressure from elevated levels. *Am J Ophthalmol*. 2016;163:132–139.e132.
94. Sigal IA, Flanagan JG, Ethier CR. Factors influencing optic nerve head biomechanics. *Invest Ophthalmol Vis Sci*. 2005;46:4189–4199.
95. Girard MJ, Suh JK, Bottlang M, Burgoyne CF, Downs JC. Scleral biomechanics in the aging monkey eye. *Invest Ophthalmol Vis Sci*. 2009;50:5226–5237.
96. Johnstone J, Fazio M, Rojananuangnit K, et al. Variation of the axial location of Bruch's membrane opening with age, choroidal thickness, and race. *Invest Ophthalmol Vis Sci*. 2014;55:2004–2009.
97. Downs JC, Burgoyne CF, Seigfreid WP, Reynaud JF, Strouthidis NG, Sallee V. 24-hour IOP telemetry in the nonhuman primate: implant system performance and initial characterization of IOP at multiple timescales. *Invest Ophthalmol Vis Sci*. 2011;52:7365–7375.
98. Fazio MA, Clark ME, Bruno L, Girkin CA. In vivo optic nerve head mechanical response to intraocular and cerebrospinal fluid pressure: imaging protocol and quantification method. *Sci Rep*. 2018;8:12639.
99. Morgan WH, Chauhan BC, Yu DY, Cringle SJ, Alder VA, House PH. Optic disc movement with variations in intraocular and cerebrospinal fluid pressure. *Invest Ophthalmol Vis Sci*. 2002;43:3236–3242.
100. Berdahl JP, Allingham RR, Johnson DH. Cerebrospinal fluid pressure is decreased in primary open-angle glaucoma. *Ophthalmology*. 2008;115:763–768.
101. Hua Y, Voorhees AP, Sigal IA. Cerebrospinal Fluid Pressure: Revisiting Factors Influencing Optic Nerve Head Biomechanics. *Invest Ophthalmol Vis Sci*. 2018;59:154–165.

Investigative Ophthalmology & Visual Science